High-Sensitivity Magnetometry Based on Quantum Beats in Diamond Nitrogen-Vacancy Centers

Kejie Fang,[1] Victor M. Acosta,[2,*] Charles Santori,[2] Zhihong Huang,[2] Kohei M. Itoh,[3] Hideyuki Watanabe,[4] Shinichi Shikata,[4] and Raymond G. Beausoleil[2]

[1]*Department of Physics, Stanford University, Stanford, California 94305, USA*
[2]*Hewlett-Packard Laboratories, 1501 Page Mill Road, Palo Alto, California 94304, USA*
[3]*Graduate School of Fundamental Science and Technology, Keio University, Yokohama 223-8522, Japan*
[4]*Diamond Research Laboratory, National Institute of Advanced Industrial Science and Technology (AIST), Tsukuba Central 2-13, 1-1-1, Umezono, Tsukuba, Ibaraki 305-8568, Japan*

(Received 16 November 2012; published 26 March 2013)

We demonstrate an absolute magnetometer based on quantum beats in the ground state of nitrogen-vacancy centers in diamond. We show that, by eliminating the dependence of spin evolution on the zero-field splitting D, the magnetometer is immune to temperature fluctuation and strain inhomogeneity. We apply this technique to measure low-frequency magnetic field noise by using a single nitrogen-vacancy center located within 500 nm of the surface of an isotopically pure (99.99% ^{12}C) diamond. The photon-shot-noise limited sensitivity achieves 38 nT/$\sqrt{\text{Hz}}$ for 4.45 s acquisition time, a factor of $\sqrt{2}$ better than the implementation which uses only two spin levels. For long acquisition times (> 10 s), we realize up to a factor of 15 improvement in magnetic sensitivity, which demonstrates the robustness of our technique against thermal drifts. Applying our technique to nitrogen-vacancy center ensembles, we eliminate dephasing from longitudinal strain inhomogeneity, resulting in a factor of 2.3 improvement in sensitivity.

DOI: 10.1103/PhysRevLett.110.130802 PACS numbers: 07.55.Jg, 76.30.Mi

Negatively charged nitrogen-vacancy (NV) centers in diamond have become an attractive candidate for solid-state magnetometry with high sensitivity and nanoscale resolution [1–4], due to their long coherence time [5] and near-atomic size. The principle of NV-based magnetometry is detection of the Zeeman shift of the ground-state spin levels. Usually, two spin levels are utilized, and the presence of a magnetic field induces a phase shift in the spin coherence which can be detected optically [6]. This scheme works well for ac (kilohertz-megahertz) magnetometry [5] and relatively low-sensitivity dc field measurements [2,4,7–10]. Sensors based on this technique are being developed for applications ranging from neuroscience [10,11], cellular biology [4,12], superconductivity [13], and nanoscale magnetic resonance imaging [14].

Recently, it was discovered that the zero-field splitting of the NV center ground state is temperature [15] and strain dependent [16]. Consequently, a magnetometer using two spin levels is subject to temperature fluctuation and strain inhomogeneity (if using an NV ensemble). This limits the magnetometer sensitivity [15,17] (for example, temperature fluctuations of 0.01 °C lead to fluctuations in the magnetometer reading of ~30 nT) and also has implications for quantum information processing [18].

In this Letter, we overcome these issues by exploiting the full spin-1 nature of the NV center [1,19–23] to observe quantum beats [24,25] in the ground state with a beat frequency given only by the external magnetic field and fundamental constants. We experimentally examined the properties of the quantum-beats scheme, based on the theoretical proposal of Ref. [1], and achieved dramatic improvement of the low-frequency sensitivity. We use a single tone microwave field, which transfers all the population into a "bright" superposition of the $m_s = \pm 1$ levels. This technique enables measurement of weak magnetic fields at the nanometer scale over a broad range of frequencies.

Quantum beating is a phenomenon of the time evolution of a coherent superposition of nondegenerate energy eigenstates at a frequency determined by their energy splitting. It has wide applications in atomic spectroscopy [26,27] and vapor-cell magnetometry [28]. The phenomenon is closely related to coherent population trapping, which has been demonstrated in many different systems including quantum dots [29,30], superconducting phase qubits [31], and NV centers [19,32].

Our quantum-beats magnetometer utilizes a linearly polarized microwave field with frequency f and transverse amplitude B_{MW} (perpendicular to the NV axis) interacting with the $S = 1$ NV ground state [Fig. 1(a)]. The Hamiltonian describing this interaction is

$$H/h = \nu_+|1\rangle\langle 1| + \nu_-|-1\rangle\langle -1| - \Omega_{R0}\cos(2\pi f t)(|1\rangle\langle 0| + |0\rangle\langle 1| + |-1\rangle\langle 0| + |0\rangle\langle -1|), \quad (1)$$

where $\Omega_{R0} = g_e\mu_B B_{\text{MW}}/\sqrt{2}$ is the undressed Rabi frequency, $\mu_B = 13.996$ GHz/T is the Bohr magneton, $g_e = 2.003$ is the NV electron g factor, h is Planck's constant, and $\nu_\pm$ is the transition frequency between $|0\rangle$ and $|\pm 1\rangle$. Here $|m_s\rangle$ denotes the ground state with spin projection $S_z = m_s$. From Eq. (1), we see that the microwave field drives transitions only between $|0\rangle$ and a certain

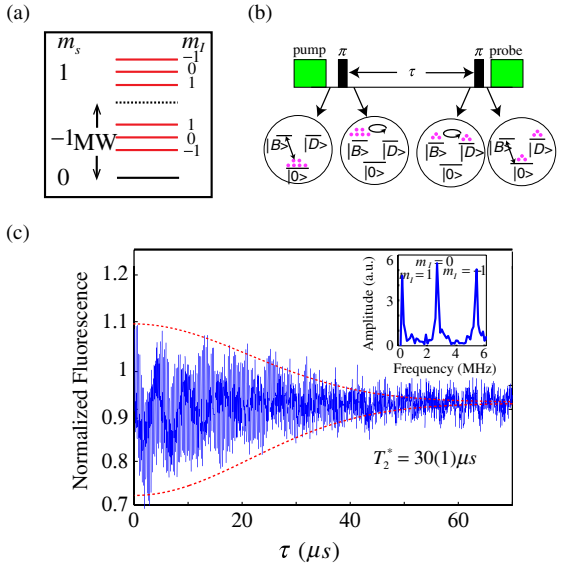

FIG. 1 (color online). (a) A single-tone microwave pulse interacts with all NV center ground-state sublevels. (b) Ramsey-type magnetometry using quantum beats between $|B\rangle$ and $|D\rangle$. (c) Ramsey fringes using the protocol in (b). The fitted decay envelope yields $T_2^* = 30(1)$ μs. Inset: Absolute value of the Fourier transform of the Ramsey fringes. The three peaks correspond to the three hyperfine resonances between $m_s = \pm 1$ levels.

superposition of $|\pm 1\rangle$, called the bright state, $|B\rangle = (|1\rangle + |-1\rangle)/\sqrt{2}$. The orthogonal superposition $|D\rangle = (|1\rangle - |-1\rangle)/\sqrt{2}$ does not interact with the microwave field and is therefore called the dark state. If $\Omega_{R0} \gg |f - \nu_\pm|$, then Eq. (1) describes the Rabi oscillation between $|0\rangle$ and $|B\rangle$, and the precession between $|B\rangle$ and $|D\rangle$ due to the difference of $\nu_\pm$ can be ignored (see Supplemental Material [33]).

Our proposed magnetometer works in the weak field and weak transverse strain regime when the transition frequencies are [16]

$$\nu_\pm \approx D + d^{\parallel}\epsilon_z \pm (g_e\mu_B B_z + A_{||}m_I), \tag{2}$$

where $D \approx 2.87$ GHz is the ground-state zero-field splitting, $d^{\parallel}$ is the axial ground-state electric dipole moment, ϵ_z is the axial electric field (crystal strain), $A_{||} = -2.16$ MHz [34] is the parallel hyperfine coefficient, and m_I is the spin projection of the ^{14}N nucleus ($I = 1$). This corresponds to the limit $|\vec{B}| \ll D/g_e\mu_B \approx 0.1$ T, $|g_e\mu_B B_z + A_{||}m_I| \gg (g_e\mu_B B_\perp + A_\perp m_I)^2/D$, and $|g_e\mu_B B_z + A_{||}m_I| \gg |d_\perp \epsilon_\perp|$, where $d_\perp$ and $\epsilon_\perp$ are the nonaxial ground-state electric dipole moment and electric field, respectively, and $A_\perp = -2.7$ MHz [35] is the perpendicular hyperfine coefficient. Note that the last condition does not set a minimum detectable magnetic field, since for usual diamond samples $d_\perp \epsilon_\perp$ is in the kilohertz range, and therefore the condition is always satisfied for at least two nuclear sublevels.

The experimental scheme, based on Ramsey interferometry, is schematically shown in Fig. 1(b). A green laser pulse initializes the NV electronic spin into $|0\rangle$. A single-tone π pulse of sufficient spectral width is then applied to transfer the spin into $|B\rangle$. After a free evolution time τ, the state becomes

$$\begin{aligned} |\psi(t)\rangle &= (e^{2\pi i\nu_+\tau}|1\rangle + e^{2\pi i\nu_-\tau}|-1\rangle)/\sqrt{2} \\ &= e^{\pi i(\nu_+ + \nu_-)\tau}\{\cos[\pi(\nu_+ - \nu_-)\tau]|B\rangle \\ &\quad + i\sin[\pi(\nu_+ - \nu_-)\tau]|D\rangle\}. \end{aligned} \tag{3}$$

We see from Eq. (3) a population evolution between $|B\rangle$ and $|D\rangle$ with a beating frequency $\nu_+ - \nu_-$. Then, a second π pulse which is phase coherent with the first π pulse projects the population in $|B\rangle$ back to $|0\rangle$, while the population in $|D\rangle$ is trapped. A final green laser pulse induces the normalized, ensemble-averaged fluorescence signal $P(\tau) \propto \{1 + F(\tau)\cos[4\pi(g_e\mu_B B_z + A_{||}m_I)\tau]\}/2$, where, for Gaussian decay, $F(\tau) \propto e^{-(\tau/T_2^*)^2}$ with T_2^* the dephasing time. By monitoring $P(\tau)$ for fixed $\tau \approx (2n+1)/[8(g_e\mu_B B_z + A_{||}m_I)]$, where n is an integer [maximizing the slope of $P(\tau)$], we can measure changes in B_z. Since $P(\tau)$ depends only on fundamental constants and B_z, the quantum-beats magnetometer is immune to temperature fluctuation and strain inhomogeneity. In principle, the magnetometer is absolute, without the need for frequent calibration; systematic errors, such as those due to transverse strain or magnetic fields (see Supplemental Material [33]), can be predicted from independently verified experimental conditions and are at the few-nT level. The offsets and drift are within an order of magnitude of those typically observed in vapor cell magnetometers [28,36,37].

In comparison, previous magnetometry demonstrations [2–5] used a large bias magnetic field such that coherence between $|0\rangle$ and only one of $|\pm 1\rangle$ was selectively addressed. Broadband magnetometry was realized by using Ramsey interferometry, which begins with a green laser pulse used to initialize the spin into $|0\rangle$, followed by a microwave $\pi/2$ pulse which creates the state $(|0\rangle + |1\rangle)/\sqrt{2}$. After a free evolution of time τ, a second $\pi/2$ pulse is applied to project the state to $|0\rangle$, which is then read out optically. The resulting fluorescence signal is $P(\tau) \propto [1 + F(\tau)\cos(2\pi\delta\tau)]/2$, where $\delta = |\nu_+ - f|$. Since δ depends on both D and ϵ_z [Eq. (2)], the measurement suffers from the temperature dependence of D [15] and inhomogeneity in ϵ_z if using an NV ensemble.

Our experiments demonstrate that overcoming these constraints is critical for high-sensitivity measurement of low-frequency magnetic fields. We used an isotopically purified ^{12}C sample ($[^{12}C] = 99.99\%$) [38] to study the temperature sensitivity of our quantum-beats magnetometer. The sample has a 500-nm-thick isotopically pure layer with $[NV] \approx 10^{11}$ cm^{-3} grown on top of a naturally abundant substrate with negligible NV density. Isotopically purified diamond samples are particularly appealing for

quantum information and sensing applications due to the long spin dephasing times afforded by the nearly spinless carbon lattice [5,18,38–41]. A homebuilt confocal microscope was used in the experiment. Light from a 532 nm laser (~ 1.2 mW) illuminated the sample through an oil-immersion objective with 1.3 numerical aperture, and the fluorescence was collected, spectrally filtered, and detected with an avalanche photodiode. Pump and probe durations were 2 and 0.3 μs, respectively. A 25 μm diameter copper wire was attached to the surface of the sample to provide square microwave field pulses with a Rabi frequency ~20 MHz.

We performed Ramsey interferometry on NV centers by using both the typical two-level scheme ($\{0, 1\}$ basis) and quantum-beats detection scheme ($\{1, -1\}$ basis). A small bias field (< 200 μT) was applied. The spin coherence time T_2^* varies among NV centers in this sample, and we chose one with relatively long T_2^*. The measured T_2^* for $\{0, 1\}$ basis and $\{1, -1\}$ basis is 62(2) and 30(1) μs, respectively [Fig. 1(c)]. From the three hyperfine resonances we find $B_z = 74.517(18)$ μT and $A_\parallel = -2.177(3)$ MHz.

Using a thermoelectric element, we varied the temperature of the diamond sample and performed $P(\tau)$ measurements using both the $\{0, 1\}$ and $\{1, -1\}$ bases. The results are plotted in Fig. 2(a). We see a clear temperature dependence in the shape of Ramsey fringes for the $\{0, 1\}$ basis which is not present in the $\{1, -1\}$ basis. We fit the data with a model containing three hyperfine levels $P(\tau) = \sum_{i=1}^{3} A_i \cos(2\pi\nu_i\tau + \phi_i) + b$, where A_i, ν_i, and ϕ_i are the amplitude, frequency, and phase of the three hyperfine oscillations, respectively, and b is a constant. We used a global fit in which $\nu_i = \nu_{i,T_0} + \Delta\nu(T)$, and A_i, ν_{i,T_0}, ϕ_i, and b are fixed for all the temperatures to fit for $\Delta\nu(T)$ [Fig. 2(b)]. For the $\{0, 1\}$ basis, assuming $\Delta\nu(T) = \Delta D(T)$, we find $dD/dT = -78(4)$ kHz/°C, which is consistent with the previous report [15]. Finally, we fixed the delay time of the Ramsey interferometer and measured the fluorescence level as the temperature was varied. As shown in Fig. 2(c), the fluorescence level in the $\{0, 1\}$ basis changed significantly and can be well fitted with the parameters obtained from fitting the temperature dependence of the Ramsey curves. In comparison, the change of fluorescence level in the $\{1, -1\}$ basis is about a factor of 7 smaller [42].

Another advantage of working in the $\{1, -1\}$ basis is the improvement of the magnetometry sensitivity by a factor of $\sqrt{2}$. Consider the minimum detectable field $b_{\min}$ of a Ramsey-type magnetometer limited by quantum-projection fluctuations. It is determined by $b_{\min} = \Delta N/(\Delta m_s g_e \mu_B |\partial N/\partial\nu|)$, where $N = \cos(2\pi\nu\tau)$ is the probability distribution difference in the two levels, ν is the spin-precession frequency in the rotating frame, ΔN is the projection noise, and Δm_s is the magnetic quantum number difference of the two levels. In both schemes we measure only the probability distribution in two levels, so we can represent the two-level system as a spin-$\frac{1}{2}$ system.

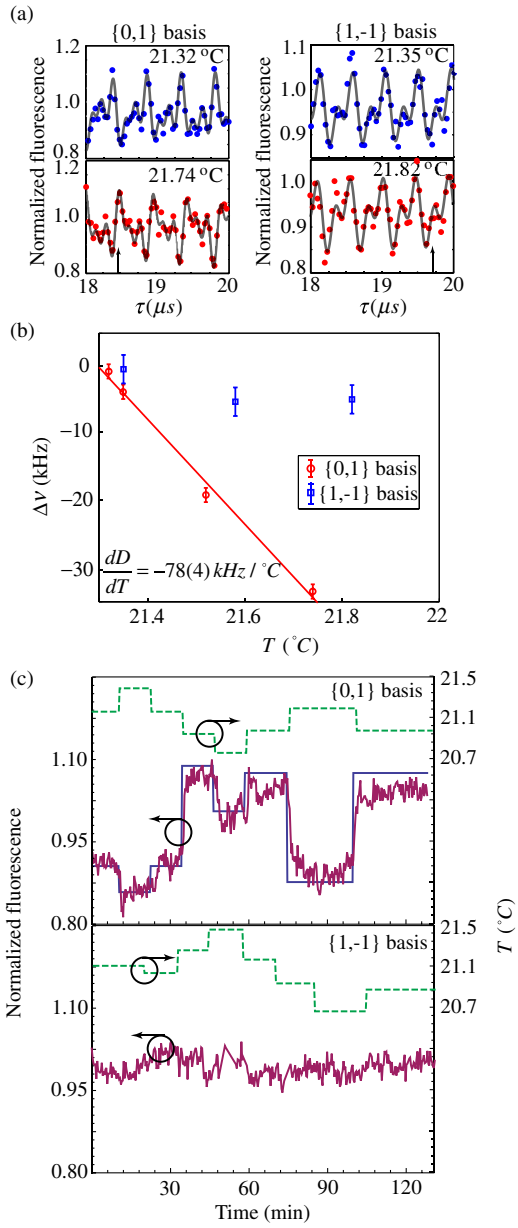

FIG. 2 (color online). (a) Ramsey fringe of the $\{0, 1\}$ basis (left panel) and $\{1, -1\}$ basis (right panel) for different temperatures. (b) Zero-field splitting D dependence on temperature as measured in the $\{0, 1\}$ basis (red). The $\{1, -1\}$ basis is immune to changing D (blue). (c) Fluorescence level dependence on temperature for fixed delay time, 18.475 μs for the $\{0, 1\}$ basis (upper panel) and 19.720 μs for the $\{1, -1\}$ basis (lower panel) [indicated by the arrows on the τ axis in (a)]. Red curves are measured data. Dashed lines indicate the temperature change. Solid lines are the calculated fluorescence level for the $\{0, 1\}$ basis.

Then the single-shot projection noise is $\Delta N = \langle \Delta\sigma_z \rangle = \sqrt{\langle\psi|\sigma_z^2|\psi\rangle - \langle\psi|\sigma_z|\psi\rangle^2}$, where σ_z is the Pauli matrix and ψ is the final state. As $\langle\psi|\sigma_z|\psi\rangle$ is simply the signal N, we have $\Delta N = |\sin(2\pi\nu\tau)|$. Inserting this expres

sion into the definition of $b_{\min}$, we find $b_{\min}(\tau) = 1/2\pi\Delta m_s g_e \mu_B C(\tau)\tau$, where $C(\tau) = e^{-(\tau/T_2^*)^2}$ is the contrast decay due to Gaussian noise. For multiple measurements, $b_{\min}$ can be improved by a factor of $\sqrt{T/\tau}$, where T is the total measurement time. The quantum-projection-noise limited sensitivity for our magnetometer is thus defined as

$$\eta_{\min}(\tau) \equiv b_{\min}\sqrt{T} = \frac{1}{2\pi\Delta m_s g_e \mu_B e^{-(\tau/T_2^*)^2}\sqrt{\tau}}. \quad (4)$$

The best sensitivity is achieved at $\tau = T_2^*/2$. Although T_2^* in the $\{1, -1\}$ basis is half of that in $\{0, 1\}$ basis, Δm_s is twice as big, so $\eta_{\min}$ is improved by a factor of $\sqrt{2}$ in the $\{1, -1\}$ basis (see Supplemental Material [33]).

In our experiment, due to finite photon collection efficiency and imperfect spin-state readout, we can measure only the photon-shot-noise limited sensitivity (see Supplemental Material [33]). However, the $\sqrt{2}$ improvement of sensitivity in the $\{1, -1\}$ basis still persists, since the contrast of $P(\tau)$ curves and photon collection efficiency are the same for the two bases. For $T = 5$ s, the optimal measured sensitivity for the $\{1, -1\}$ basis and $\{0, 1\}$ basis is 38(3) and 53(4) nT/$\sqrt{\text{Hz}}$, respectively. The ratio of the two sensitivities is 1.39(15), which is consistent with the theoretical value of $\sqrt{2}$. In comparison, the quantum-projection-noise limited sensitivity calculated by using Eq. (4) is 0.79 and 1.12 nT/$\sqrt{\text{Hz}}$, respectively (we used the conversion $\sqrt{\text{s}} \leftrightarrow \sqrt{2}/\sqrt{\text{Hz}}$).

We used both schemes to measure the real noise in the laboratory. Using $\tau = 14.5$ μs (29 μs) for the $\{1, -1\}$ ($\{0, 1\}$) basis, we repeated the fluorescence measurement in 1-s intervals for 50 min, now without any active temperature control. As seen from Fig. 3(a), for frequencies near 1 Hz, the noise floor measured by the $\{1, -1\}$ and $\{0, 1\}$ bases is 50(1) and 61(2) nT/$\sqrt{\text{Hz}}$, respectively. If we ignore dead time from state preparation and readout, the sensitivity is 43(1) and 56(2) nT/$\sqrt{\text{Hz}}$, respectively, consistent with the photon-shot-noise limit. For lower frequencies, the $\{0, 1\}$ basis suffers more noise which is presumably due to laboratory temperature fluctuations.

To further elucidate this effect, we analyzed the two-sample Allan deviation [43] of the fluorescence data, as shown in Fig. 3(b). The Allan deviation in the $\{0, 1\}$ basis at long gate time (T_{gate}) levels off and even begins to increase at $T_{\text{gate}} \sim 100$ s, indicating that averaging the signal for a longer period of time no longer improves estimation of a static magnetic field. In contrast, the Allan deviation continues to decrease for the $\{1, -1\}$ basis up to $T_{\text{gate}} \geq 1000$ s, indicating that this technique is suitable for distinguishing nT-scale static fields by using long integration times. This stability of Allan deviation means that our magnetometer does not require recalibration when the environment condition changes.

Finally, we studied the effect of strain inhomogeneity on a magnetometer employing an ensemble of NV centers. We expect that, from Eq. (2), $P(\tau)$ measurement in the $\{1, -1\}$ basis is insensitive to strain inhomogeneity; however, there will be inhomogeneous broadening, and consequently reduction of T_2^*, in the $\{0, 1\}$ basis due to variations in ϵ_z for each NV center in the ensemble. We used a sample with $[^{12}\text{C}] = 99.9\%$, which was implanted with $10^{10}/\text{cm}^2$ $^{14}\text{N}^+$ at an energy of 20 keV and annealed at 875 °C for 2 h, resulting in an NV density of $\sim 5/\mu\text{m}^2$. The laser spot was defocused to illuminate a ~ 2.5 μm diameter region, and the optical power was increased to 30 mW to maintain constant intensity. A bias field $B_z \approx 28$ μT was applied along the [100] direction, such that NVs with different orientation experience the same $|B_z|$. For the $\{1, -1\}$ basis, we used microwave pulses with enough spectral width to cover all three hyperfine levels. For the $\{0, 1\}$ basis, we detuned the microwave frequency and reduced the power to selectively address the $m_I = -1$ level. The peak corresponding to the $m_I = -1$ level of the Fourier transform of $P(\tau)$ is shown in Fig. 4 for both cases. Gaussian fits revealed a full width at half maximum $\Gamma = 0.09(1)$ and 0.12(2) MHz for the $\{1, -1\}$ and $\{0, 1\}$ bases, respectively. This indicates a factor of $\sim 2.7(7)$ increase in spin linewidth due to inhomogeneous broadening in the $\{0, 1\}$ basis, since for a single NV Γ would be half of that of the $\{1, -1\}$ basis. Accordingly, we estimate that the longitudinal strain inhomogeneity in the detected

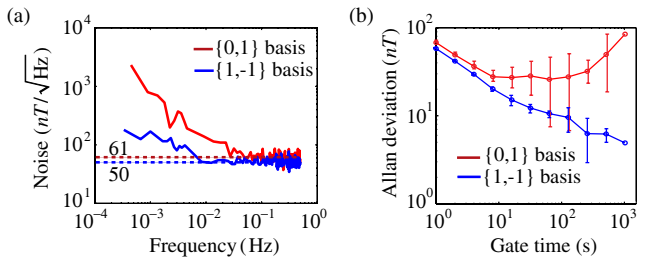

FIG. 3 (color online). (a) Measured noise spectrum using the $\{0, 1\}$ and $\{1, -1\}$ bases. Dashed lines are the noise floor near 1 Hz. (b) Allan deviation of the noise.

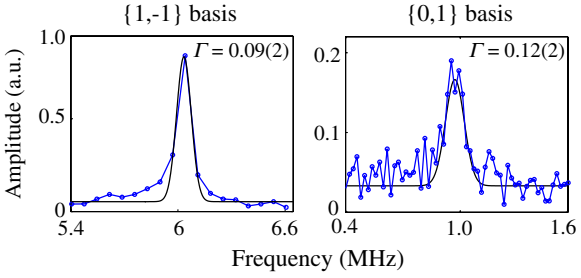

FIG. 4 (color online). Fourier transform of $P(\tau)$ in both bases for an ensemble of NV centers. Each peak corresponds to the $m_I = -1$ level. Black curves are Gaussian fits.

region is ~100 kHz. The result indicates a factor of 2.3(3) improvement of sensitivity for the quantum-beats magnetometer according to Eq. (4). Our result also sheds light on other NV-ensemble applications such as quantum memories [44,45] and frequency references [46].

In summary, we have demonstrated a broadband magnetometer insensitive to temperature fluctuation and strain inhomogeneity based on quantum beats in NV centers in diamond. Although slow temperature drifts are eliminated in ac magnetometry by using two levels, our scheme should eliminate errors due to dynamic temperature changes from laser and microwave pulses [18]. Also, the new method uses a similar pulse sequence and does not increase the complexity of the magnetometer.

We thank D. Budker, B. Patton, P. R. Hemmer, K.-M. C. Fu, and T. Ishikawa for contributing valuable ideas during the conception of this experiment. K. F. acknowledges the support of S. Fan.

*victor.acosta@hp.com

[1] J. M. Taylor, P. Cappellaro, L. Childress, L. Jiang, D. Budker, P. R. Hemmer, A. Yacoby, R. Walsworth, and M. D. Lukin, Nat. Phys. **4**, 810 (2008).
[2] J. R. Maze *et al.*, Nature (London) **455**, 644 (2008).
[3] C. L. Degen, Appl. Phys. Lett. **92**, 243111 (2008).
[4] G. Balasubramanian *et al.*, Nature (London) **455**, 648 (2008).
[5] G. Balasubramanian *et al.*, Nat. Mater. **8**, 383 (2009).
[6] A. Gruber, A. Dräbenstedt, C. Tietz, L. Fleury, J. Wrachtrup, C. von Borczyskowski, Science **276**, 2012 (1997).
[7] L. Rondin, J.-P. Tetienne, P. Spinicelli, C. D. Savio, K. Karrai, G. Dantelle, A. Thiaville, S. Rohart, J.-F. Roch, and V. Jacques, Appl. Phys. Lett. **100**, 153118 (2012).
[8] P. Maletinsky, S. Hong, M. S. Grinolds, B. Hausmann, M. D. Lukin, R. L. Walsworth, M. Loncar, and A. Yacoby, Nat. Nanotechnol. **7**, 320 (2012).
[9] V. M. Acosta, E. Bauch, A. Jarmola, L. J. Zipp, M. P. Ledbetter, and D. Budker, Appl. Phys. Lett. **97**, 174104 (2010).
[10] L. M. Pham *et al.*, New J. Phys. **13**, 045021 (2011).
[11] L. T. Hall *et al.*, Sci. Rep. **2**, 401 (2012).
[12] L. P. McGuinness *et al.*, Nat. Nanotechnol. **6**, 358 (2011).
[13] L.-S. Bouchard, V. M Acosta, E. Bauch, and D. Budker, New J. Phys. **13**, 025017 (2011).
[14] M. S. Grinolds *et al.*, arXiv:1209.0203.
[15] V. M. Acosta, E. Bauch, M. P. Ledbetter, A. Waxman, L.-S. Bouchard, and D. Budker, Phys. Rev. Lett. **104**, 070801 (2010).
[16] F. Dolde *et al.*, Nat. Phys. **7**, 459 (2011).
[17] D. M. Toyli, D. J. Christle, A. Alkauskas, B. B. Buckley, C. G. Van de Walle, and D. D. Awschalom, Phys. Rev. X **2**, 031001 (2012).
[18] P. C. Maurer *et al.*, Science **336**, 1283 (2012).
[19] E. Togan *et al.*, Nature (London) **466**, 730 (2010).
[20] F. Shi *et al.*, Phys. Rev. Lett. **105**, 040504 (2010).
[21] P. Huang, X. Kong, N. Zhao, F. Shi, P. Wang, X. Rong, R.-B. Liu, and J. Du, Nat. Commun. **2**, 570 (2011).
[22] F. Reinhard *et al.*, Phys. Rev. Lett. **108**, 200402 (2012).
[23] X. Xu *et al.*, Phys. Rev. Lett. **109**, 070502 (2012).
[24] F. G. Major, *The Quantum Beat: Principles and Applications of Atomic Clocks* (Springer, New York, 2007).
[25] M. Auzinsh and R. Ferber, *Optical Polarization of Molecules* (Cambridge University Press, Cambridge, England, 1995).
[26] S. Haroche, in *High-Resolution Laser Spectroscopy*, edited by K. Shimoda (Springer, Berlin, 1976), pp. 256–313.
[27] J. N. Dodd and G. W. Series, in *Progress in Atomic Spectroscopy*, edited by W. Hanle and H. Kleinpoppen (Plenum, New York, 1978), Vol. 1, pp. 639–677.
[28] S. J. Seltzer, P. J. Meares, and M. V. Romalis, Phys. Rev. A **75**, 051407(R) (2007).
[29] B. Michaelis, C. Emary, and C. W. J. Beenakker, Europhys. Lett. **73**, 677 (2006).
[30] X. Xu, B. Sun, P. R. Berman, D. G. Steel, A. S. Bracker, D. Gammon, and L. J. Sham, Nat. Phys. **4**, 692 (2008).
[31] W. D. Kelly, Z. Dutton, J. Schlafer, B. Mookerji, T. A. Ohki, J. S. Kline, and D. P. Pappas, Phys. Rev. Lett. **104**, 163601 (2010).
[32] C. Santori *et al.*, Phys. Rev. Lett. **97**, 247401 (2006).
[33] See Supplemental Material at http://link.aps.org/supplemental/10.1103/PhysRevLett.110.130802 for extra theoretical analysis.
[34] B. Smeltzer, J. McIntyre, and L. Childress, Phys. Rev. A **80**, 050302 (2009).
[35] S. Felton, A. Edmonds, M. Newton, P. Martineau, D. Fisher, D. Twitchen, and J. Baker, Phys. Rev. B **79**, 075203 (2009).
[36] V. M. Acosta, M. Ledbetter, S. Rochester, D. Budker, D. J. Kimball, D. Hovde, W. Gawlik, S. Pustelny, J. Zachorowski, and V. Yashchuk, Phys. Rev. A **73**, 053404 (2006).
[37] D. Budker *et al.*, in *Optical Magnetometry* (Cambridge University Press, Cambridge, England, 2013), Chap. 20.
[38] T. Ishikawa, K.-M. C. Fu, C. Santori, V. M. Acosta, R. G. Beausoleil, H. Watanabe, S. Shikata, and K. M. Itoh, Nano Lett. **12**, 2083 (2012).
[39] K. Ohno *et al.*, Appl. Phys. Lett. **101**, 082413 (2012).
[40] N. Zhao *et al.*, Nat. Nanotechnol. **7**, 657 (2012).
[41] K. D. Jahnke, B. Naydenov, T. Teraji, S. Koizumi, T. Umeda, J. Isoya, and F. Jelezko, Appl. Phys. Lett. **101**, 012405 (2012).
[42] If we attribute the fluctuation of the fluorescence level of the $\{1, -1\}$ basis to a temperature-dependent resonance frequency shift, then by correlating the fluorescence level in Fig. 2(c) with the temperature changes, we find $d\Delta\nu/dT = 1.4(4)$ kHz/°C in the $\{1, -1\}$ basis, which corresponds to a magnetometer reading fluctuation of 0.25(7) nT for a temperature change of 0.01 °C.
[43] D. W. Allan, Proc. IEEE **54**, 221 (1966).
[44] Y. Kubo *et al.*, Phys. Rev. Lett. **105**, 140502 (2010).
[45] Zhu *et al.*, Nature (London) **478**, 221 (2011).
[46] J. S. Hodges and D. Englund, arXiv:1109.3241.